Conical Shock-Wave Turbulent Boundary-Layer Interaction Including Suction Effects

WILLIAM R. SEEBAUGH* AND MORRIS E. CHILDS†
University of Washington, Seattle, Wash.

An experimental apparatus was designed to produce shock-wave boundary-layer interactions representative of those occurring on the cowl surfaces of axially symmetric inlets with supersonic internal compression. Provision was made for boundary-layer removal through normal perforations located upstream of or within the regions of shock-wave boundary-layer interaction. Data were obtained for adiabatic wall conditions at freestream Mach numbers of 2.82 and 3.78. Flowfield and boundary-layer properties obtained upstream of, within, and downstream of the interaction regions are presented for several shock-wave strengths and suction flow rates. The results for conical incident shock waves show that the boundary layers separated at lower incident shock-wave strengths than previously observed for two-dimensional flow. It was also observed that a separated region as long as two boundary-layer thicknesses in extent could be eliminated by removing about 3% of the boundary-layer mass flow from the interaction region, and that suction within the interaction region was more effective in controlling separation than suction upstream of the shock-impingement location.

Nomenclature

L = length of interaction region
$\dot{m}_B$ = suction (bleed) mass-flow rate
$\dot{m}_{BL}$ = boundary-layer mass-flow rate
M = Mach number
N_L = power-law exponent for minimum least-square error on logarithmic plot of velocity ratio vs height
N = power-law exponent for which the mass-flow rate in the boundary layer is equal to the measured mass-flow rate
P = static pressure
R = duct radius
Re = Reynolds number
U = axial velocity component
x = axial coordinate
y = radial coordinate, measured from wall
α_1 = flow-deflection angle across incident shock wave (two-dimensional value for conical shock waves)
δ = boundary-layer thickness
δ^* = boundary-layer displacement thickness

Subscripts

1 = upstream limit of interaction region
3 = downstream limit of interaction region
e = boundary-layer edge
0 = tunnel reference condition
t = total conditions
∞ = freestream

1. Introduction

WHEN shock-wave turbulent boundary-layer interactions occur in a duct, such as a supersonic diffuser, the secondary flowfields induced by the interactions may have a large influence on the performance of the device, particularly if flow separation occurs. It has been observed experimentally that the boundary layers near the throat regions of supersonic diffusers can extend completely across the ducts at freestream Mach numbers above about 5. Relatively thick boundary layers can also be expected in small inlet models when the freestream Reynolds numbers are much lower than those for the full-scale flight conditions, compounding the difficulty of extrapolation of test-model data. Predictions of shock-wave boundary-layer interaction characteristics for two-dimensional and axially symmetric flows[1] indicate that the changes in boundary-layer properties across the interaction region are larger for conical incident shock waves in axially symmetric flow and that the differences become significant when the ratio of boundary-layer height upstream of the interaction region to duct radius is greater than about 0.1. The predicted static-pressure increase across the region of interaction for the viscous case in axially symmetric flow is also larger than that associated with a simple inviscid shock reflection. These observations suggest the possibility that conical incident shock waves interacting with relatively thick boundary layers in circular ducts could cause flow separation at shock strengths lower than those reported by Kuehn for two-dimensional flow.[2]

The adverse effects of boundary-layer separation may be suppressed by removing a portion of the low-energy flow from the interaction region. Predictions of the effects of boundary-layer suction on the changes in boundary-layer characteristics across shock-wave turbulent boundary-layer interactions are given in Ref. 1. The influence of suction on shock-wave boundary-layer interactions was investigated experimentally by Strike and Rippey,[3] Kutschenreuter et al.,[4] and Wainwright[5] using two-dimensional test models with various perforated-plate suction surfaces. The results of these studies indicated that separation could be eliminated by removing a sufficient portion of the boundary-layer flow; however, for Refs. 3 and 4 the perforated plates that were used in the studies extended far upstream of the interaction region. The effects of the location of the suction surface relative to the shock-impingement point were considered in the study reported in Ref. 5, but quantitative results were not given. Detailed data for suction concentrated within the interaction region, as considered in the flow models of Ref. 1, were not available when the present study was initiated.

Presented as Paper 69-450 at the AIAA 5th Propulsion Joint Specialist Conference, U.S. Air Force Academy, Colorado, June 9–13, 1969; submitted June 9, 1969; revision received November 26, 1969. This paper is based on a dissertation submitted by the senior author in partial fulfillment of the requirements of the degree of Doctor of Philosophy. The work was supported by NASA Grant NGR-48-002-047, under administration of the Air-breathing Propulsion Branch, Ames Research Center.

* Predoctoral Research Associate, Mechanical Engineering; presently, Senior Systems Engineer, Fairchild-Hiller Corporation, Republic Aviation Division, Farmingdale, N. Y. Member AIAA.

† Professor, Mechanical Engineering. Member AIAA.

1.1 Experimental Objectives

The experimental investigation described in this paper was conducted in order to obtain basic data on the interaction of a conical shock wave and a turbulent boundary layer. The experimental configuration was considered to be particularly suitable for the investigation of shock-wave boundary-layer interaction phenomena because the three-dimensional secondary flows associated with the corners and sidewalls of two-dimensional wind tunnels and test models were completely eliminated. The primary emphasis was placed on the determination of differences between the present axially symmetric flow and the corresponding two-dimensional flows studied by previous investigators, and on the effects of suction on the interaction-region characteristics and the occurrence of flow separation.

1.2 Apparatus

The experimental apparatus was a steady-flow wind tunnel that consisted of a transparent plastic converging-diverging nozzle with exit diameter of 2.030 in., a conical metal centerbody, and a constant diameter transparent plastic test section (Fig. 1). The contours of the axially symmetric nozzles were designed by the method of characteristics. Two nozzles with nominal exit Mach numbers of 3 and 4 were constructed. The starting properties for the characteristics calculations were obtained by specifying parabolic wall contours in the throat region and assuming conical source flow to a Mach number of 1.127 for the Mach 3 nozzle and to 1.145 for the Mach 4 design. The characteristics nets were carried out to Mach numbers of 2.94 and 3.95, respectively, for the Mach 3 and 4 nozzles.

The test sections consisted of transparent plastic tubes of constant inner diameter (2.030 in.), axial segments of which could be enclosed by an interchangeable outer ring (Fig. 2). After completing the tests with solid tunnel walls, circumferential rows of 0.064-in.-diam bleed holes were drilled into the test section as shown. A maximum porosity of 42% over a length of 0.275 in. was obtained with 228 holes in four rows around the section. The slot around the outside of the section provided the volume required for the bleed plenum chamber. The lines connecting the test section to the suction flow metering and pumping system were attached to the bleed-collection ring.

The centerbody configuration consisted of a common rear support section with interchangeable conical tips on the upstream end. The centerbody served as the shock-wave generator and also as the forward portion of the wind-tunnel diffuser. A sharp corner was provided at the end of each cone in order to allow clear definition of the regions of the flow that were influenced by the change in body slope. The axial position of the tip of the centerbody could be changed to allow a continuous variation in the shock-impingement location on the wall. The centerbody was held at the center of the test section by four support pins located downstream of the cone base. A second set of supports at the aft end of the subsonic diffuser was used to align the centerbody axis parallel to the tunnel axis.

1.3 Instrumentation and Data Reduction

Tunnel parameters

The tunnel total pressure was measured by means of a static pressure orifice located in the plenum chamber wall. Total pressures below 40 psi (atmospheric reference) were read on a mercury manometer, and higher values were read on a pressure gage. The maximum error in the tunnel total pressure was estimated to be about 0.7% of the reading. The tunnel plenum (total) temperature was measured with an unshielded iron-constantan thermocouple. The estimated maximum error in the total temperature measurement was 1% of the absolute temperature.

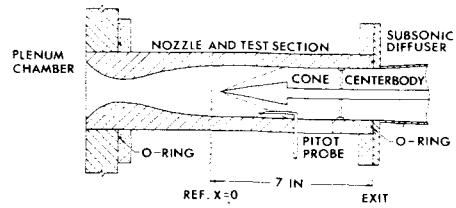

Fig. 1 Wind-tunnel nozzle.

Surface static pressure

Twenty-five 0.0135-in.-diam static-pressure orifices with spacing varying from 0.05 to 0.20 in. were installed in a single row in each test section, with a dense distribution near the theoretical shock-impingement location. Three additional pairs of orifices were located at 90° intervals around the circumference to aid in symmetry verification. The orifices were connected to an absolute strain-gage pressure transducer with a range of 0–10 psia by lengths of stainless steel and plastic tubing. The output of the transducer was read on a precision null potentiometer. The same instrumentation was used for measurement of the static pressures at the inlet and throat of the suction flow-metering nozzle. The maximum error for the static pressures, including potentiometer error, was about 2% of the reading.

Pitot probe surveys

Pitot-pressure measurements were obtained using a long curved probe with a flattened tip connected to a differential strain-gage pressure transducer with a range of ±25 psi (atmospheric reference). The transducer output was read on a potentiometer. The maximum error after conversion to absolute pressure was about 3% of the absolute reading. The probe-tip opening was 0.003-in. high and 0.017-in. wide, and the over-all height of the tip of the probe was 0.008 in. Pitot pressure profiles were obtained at the centerline positions of the surface static-pressure orifices. The distance between surveys was either 0.1 or 0.2 in.

Mach numbers were calculated from the ratio of Pitot pressure to surface static pressure for all points on the profiles. The distance from the wall to the freestream was defined as the transverse coordinate of the point at which the Mach number was just equal to or greater than 0.999 times the value at the next point on the profile. In a similar manner, the boundary-layer thickness δ for each profile was set equal to the coordinate at which the Mach number was just equal to or greater than 0.99 times the freestream Mach number. No interpolation between points on the profiles was performed to determine the point at exactly 0.99 M_∞, since the spacing between data points was sufficiently small (0.005 in.) to guarantee acceptable accuracy with the method used. The test-section freestream Mach number for the nominal Mach 3 nozzle was 2.82, and the variation from this value across the entire test section was ±0.7%. The test section Mach number for the nominal Mach 4 nozzle was 3.78 with a variation of ±1.2%. A second value of Mach number for points outside of the boundary layer was calculated from the ratio of Pitot pressure to the local freestream total pressure. An estimate of the

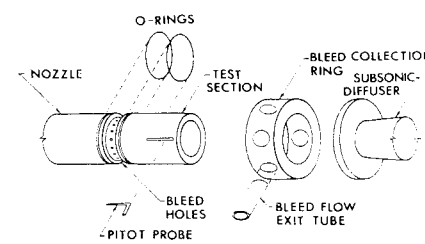

Fig. 2 Wind-tunnel test section.

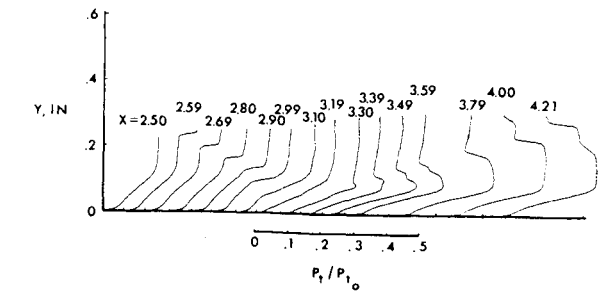

a) Pitot pressure surveys

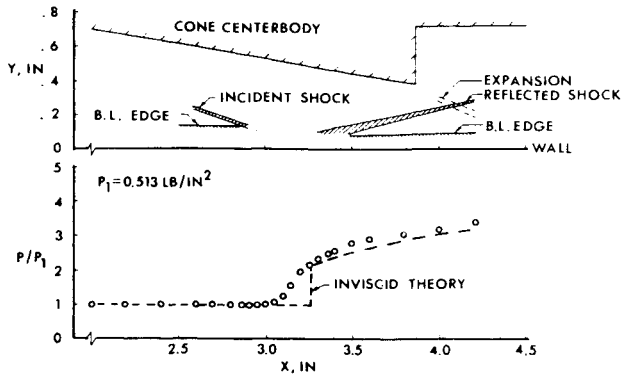

b) Flowfield and surface static-pressure distribution

Fig. 3 Results for 10° cone at $M_\infty = 3.78$.

local freestream total pressure downstream of an interaction region was obtained from the product of the tunnel total pressure and the theoretical total pressure recovery across the incident and reflected shock waves. The two Mach number curves were nearly coincident outside of the boundary layer for profiles not within regions of shock-wave boundary-layer interaction, indicating that the variations in static pressure across the boundary layer were small for those profiles.

Boundary-layer velocity profiles and integral properties were determined from the Mach number distributions, assuming constant static pressure and total temperature across the boundary layer. A best-fit power-law exponent N_L was obtained by computing the straight line of minimum least-square error on a logarithmic plot of U/U_e vs y/δ. A second power-law exponent N was determined by matching the mass flow of the power-law profile to the measured value.

Boundary-layer suction flow

The boundary-layer suction mass-flow rate was measured using a long-radius flow nozzle that was constructed according to ASME standards.[6] The nozzle was calibrated in place by metering the flow with a previously calibrated square-edged orifice. The total temperature of the suction flow was measured with an unshielded iron-constantan thermocouple. The nozzle used had a lower resolution limit of 0.002 lb_m/sec, and an estimated maximum error of ±5% of the measured flow rate.

2. Results and Discussion

Experimental results are presented in the form of Pitot pressure surveys, surface static pressures, velocity profiles, flowfield patterns determined from analysis of the Pitot pressure surveys and surface static-pressure profiles, and boundary-layer thickness and integral properties. Pitot pressure survey stations and static pressure orifice locations are identified by the distance in inches downstream of a zero reference station 7.0 in. upstream of the entrance to the subsonic diffuser. The range of survey locations was from 2.40 to 4.21 in.

2.1 Solid Wall Tests

Measurements with solid tunnel walls were made at Mach numbers of 2.82 and 3.78. The tunnel total pressures were selected to give approximately equal values of Re_δ at $x = 3.3$ in., which was the theoretical shock-impingement point. The resulting unit Reynolds number was 5.6×10^6 ft^{-1}, and the Reynolds number based on the boundary-layer thickness of 0.138 in. (average of several tests) just upstream of the interaction region was about 6×10^4 for both Mach numbers. With a duct radius of 1.015 in., the average ratio δ_1/R was 0.136. The half-angle of the conical shock-wave generator was varied to give a range of incident shock strengths corresponding to flow-deflection angles from approximately 2° to 9°. Typical results obtained at $M_\infty = 3.78$ are discussed in the following paragraphs.

Surface pressures and Pitot surveys

Pitot pressure profiles taken upstream of, within, and downstream of the interaction region for a 10° cone at $M_\infty = 3.78$ are shown in Fig. 3a. The profile obtained at $x = 2.59$ shows the edge of the boundary layer and the incident shock wave, which appears as a near-discontinuity about 0.01 in. thick. The Pitot pressure increases rapidly as the probe moves above the shock wave into a region of lower Mach number. The incident shock wave is also defined on the four subsequent profiles. The rapid pressure decreases in the y direction for profiles downstream of $x = 3.30$ in. define the reflected shock wave. This pressure rise initially occurs in two steps (see profiles at $x = 3.49$ in. and 3.59 in.); however, the waves coalesce within a short distance. At $x = 4.00$ in. the Pitot pressure decreases as the probe moves above the shock wave into a higher Mach number region, remains nearly constant in the conical flow, and then decreases again through the region of increasing Mach number within the expansion originating at the base of the cone. The Pitot pressure approaches the cone base pressure when the probe is directly behind the cone. The corner expansion waves cross the reflected shock wave between $x = 4.00$ in. and 4.21 in.

The wave patterns, the measured boundary-layer thickness upstream of the incident shock wave and downstream of the reflected shock wave, and the measured surface static-pressure distribution are given in Fig. 3b for the 10° cone. As shown by the profiles from $x = 2.99$ in. to 3.19 in., the boundary layer merged continuously with the conical flow within the interaction region and the boundary-layer thickness could not be defined for these profiles. The pressure distribution is compared to that obtained by a method-of-characteristics calculation. The flow pattern and pressure distribution exhibit typical characteristics of a weak unseparated interaction.[7] The incident and reflected shock waves are distinct and the measured surface static pressures spread about one boundary-layer thickness forward of the theoretical pressure rise.

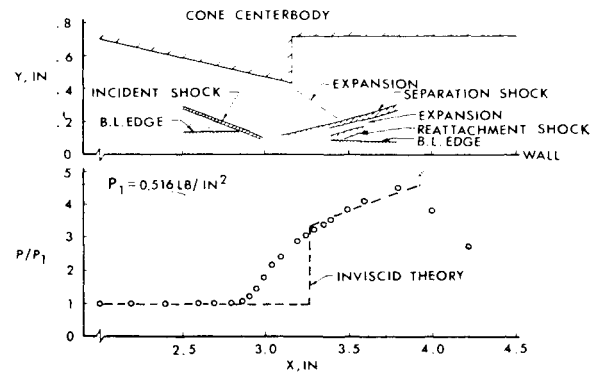

Fig. 4 Flowfield and surface static-pressure distribution for 13° cone at $M_\infty = 3.78$.

The pressure discontinuity of the inviscid distribution, which was computed for the nominal cone half-angle (10°), was located at the intersection of the projection of the measured incident shock wave and the wall and corresponds to a flow-deflection angle through the conical incident shock wave of 4.3°. The flow-deflection angle was also determined by measuring the wave angle of the incident shock wave from the locations on the Pitot profiles, and by determining the Mach number from the tunnel total pressure and the Pitot pressure behind the shock wave with consideration given to the total pressure loss across the shock wave. The results were 3.7° and 4.7°, respectively, giving an apparent uncertainty of ±0.5 degrees about the nominal value. Because of this uncertainty, the nominal shock-wave strength is used in all further descriptions and for the comparisons of analytical and experimental results.

Certain characteristics of separated flow are exhibited by the flowfield and surface static-pressure distribution for a 13° cone [(7.2° deflection angle at $M_\infty = 3.78$ (Fig. 4)]. Comparison to Fig. 3 shows that the wave pattern downstream of the interaction region is more complex for the stronger incident shock wave. The appearance of a separation shock wave is consistent with the increase in the spreading of the surface static-pressure rise to about 3.3 boundary-layer thicknesses upstream of the projected intersection of the incident shock and the wall. This pressure rise causes a rapid thickening of the subsonic part of the boundary layer which leads to the formation of an effective compression surface for the supersonic part of the flow and the formation of the separation shock wave. This shock wave is followed by a left-running expansion that is followed in turn by a second shock wave. This multiple-shock pattern, without rapid coalescence of the compression waves, is typical of those shown in schlieren photographs of separated two-dimensional interactions.[7]

The separated-flow region for the 13° cone was apparently very small since the Pitot pressure surveys did not indicate a reversed flow region of measurable extent. The surface static-pressure distribution shows only a long region of nearly constant pressure gradient, and not the characteristic "hump" generally observed for separated two-dimensional interactions.[2] The decrease in surface static-pressure downstream of $x = 3.8$ is caused by the expansion from the base corner of the cone. The boundary-layer data at $x = 3.79$ were influenced by the interaction of the expansion with the reflected waves and the boundary layer itself. The influence of the expansion on the occurrence of the multiple-shock pattern and the boundary-layer properties upstream of $x = 3.7$ is believed to be negligible.

The highest cone angle tested at $M_\infty = 3.78$ was 15°, which gave a flow-deflection angle equal to 9.2° (Fig. 5). For a shock of this strength, the static-pressure distribution exhibits a hump typical of those used as an indication of the presence of a separated flow region in two-dimensional flow.[2] Because

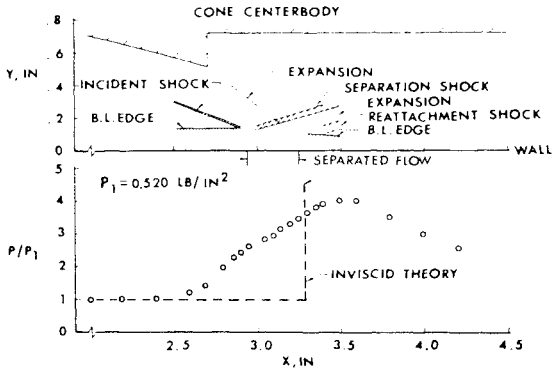

Fig. 5 Flowfield and surface static-pressure distribution for 15° cone at $M_\infty = 3.78$.

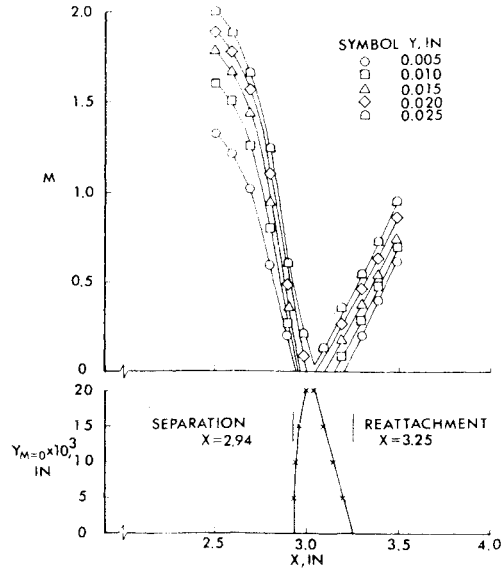

Fig. 6 Determination of separation and reattachment points, 15° cone at $M_\infty = 3.78$.

of the small cone diameter (a result of tunnel blockage limitations) the expansion from the base of the cone reached the boundary layer very near the end of the interaction region. The pressure decrease associated with the expansion was not large enough to affect the occurrence of separation; however, the boundary-layer properties downstream of $x = 3.3$ were influenced by the interaction of the expansion with the reflected wave system and the boundary layer.

Approximate separation and reattachment points were determined by plotting the Mach number variations vs the axial coordinate at fixed distances from the wall (Fig. 6). The intersections of lines of constant y with the $M = 0$ axis were cross plotted and extrapolated to $y = 0$. The upstream and downstream intersections of the extrapolated curves with the wall were identified, respectively, as the separation and reattachment points. The separated region between these points, shown on Fig. 5, brackets three profiles that indicated reversed flow at $y = 0.005$ in. ($x = 2.99 - 3.19$ in.).

Boundary-layer properties

Typical boundary-layer velocity profiles are shown in Fig. 7. The dashed lines passing through the data points correspond to the best-fit profiles with profile exponent N_L. This profile reflects the minimum least-square error on a logarithmic scale. The solid lines represent the power-law profiles with exponent N giving the measured boundary-layer mass flux. The close agreement between the data points and the power-law profiles for the upstream data indicates that the power law gives a good representation of the turbulent boundary-layer velocity distribution for these profiles. This agreement can be made arbitrarily close by reducing the number of points on the profiles, that is, by choosing the boundary-layer edge at a lower value of M_e/M_∞. This procedure, however, results in reductions in the displacement thickness for ratios less than 0.99, indicating that 0.99 is very close to the proper value when correlations are based on displacement thickness.

The second set of profiles was obtained near the end of the interaction region for the 10° and 15° cones. The profile is somewhat distorted for the 10° cone, but is still well-represented by the power-law profiles. For the 15° cone, however, the power-law profiles are less representative of the actual profile shape.

The third pair of profiles was obtained relatively far downstream of the interaction region for the 10° cone, and just

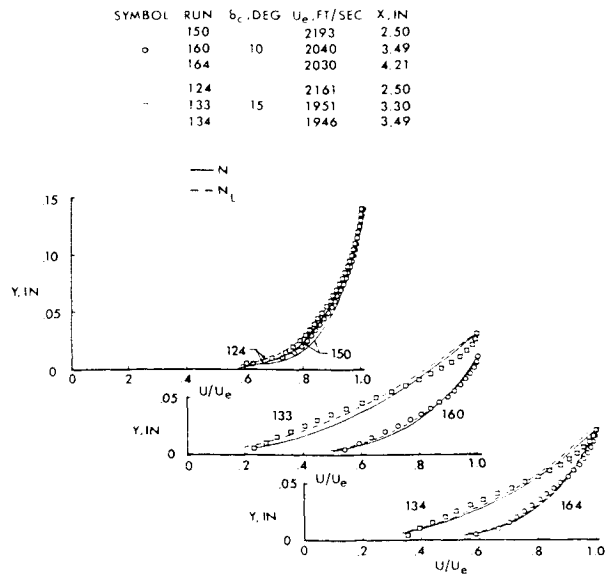

Fig. 7 Boundary-layer velocity distributions, $M_\infty = 3.78$.

downstream of reattachment for the 15° cone. These profiles are not similar to the upstream profiles, and have developed inflection points that cannot be represented by power laws.

The streamwise variations in measured boundary-layer properties are shown in Fig. 8 for the 10°, 13°, and 15° cones. As discussed previously, no boundary-layer properties were defined within the interaction regions. An "effective" boundary-layer thickness would decrease monotonically between the upstream and downstream thicknesses for the unseparated case (10° cone), whereas a peaked thickness distribution is typical of the stronger interactions.[7] The boundary-layer downstream of the interaction region was not influenced by the expansion from the base of the cone for the 10° case. The results indicate that the additional compression in this region retards the redevelopment of an equilibrium boundary-layer profile. The displacement thickness downstream of the interaction region is larger for the 13° and 15° cones. This trend of increasing thickness parameters for high-strength shocks was also observed for two-dimensional flow[8] as was the continued decrease in power-law exponent with increasing shock strength (Fig. 8). For the 15° cone, all integral properties downstream of the interaction region were influenced by the expansion from the base of the cone.

Incipient separation

The conditions for incipient separation for two-dimensional and axially symmetric flows are compared in Fig. 9 in terms of the flow-deflection angles through the incident shock waves and the pressure ratios across the interaction regions. The curves for two-dimensional flow are cross plots of data reported by Kuehn[2] and correspond to the over-all pressure ratio existing just before the first appearance of a hump in the surface static-pressure distribution at each Reynolds number. The values of α_1 for incipient separation obtained during the present study are the deflection angles associated with the highest cone angles without separated flow at each Mach number, as indicated by the static-pressure distributions and the occurrence of regions of constant Pitot pressure near the wall. The downstream pressure P_3 is the surface static pressure at the station where the last identifiable compression wave leaves the edge of the boundary layer. Since the downstream end of the reflected wave system is rather indistinct, the selection of P_3 is somewhat arbitrary.

The comparisons shown in Fig. 9 clearly show that the boundary layer separated at lower values of α_1 for the conical shock waves. This result is attributed primarily to the larger pressure ratio across the interaction region for the axially symmetric flow at a given value of α_1.

The influence of the respective test facilities and data reduction procedures on the comparisons in Fig. 9 should be small since the model sizes, instrumentation locations, and boundary-layer thicknesses for the two experiments were nearly identical. The boundary-layer edge Mach number was equal to 0.99 times the freestream value for both experiments, and the same methods of detecting separation were used.

2.2 Perforated-Wall Tests

Various perforation patterns were obtained by successively adding bleed holes in rows around the test section, beginning with one row of 54 0.064-in.-diam holes. The location of the incident shock wave was 0.4 in. upstream from the position used in the solid-wall tests. Perforated-wall test data are presented for the 15° cone.

Surface-pressures and Pitot surveys

A suction flow rate equal to 3.1% of the upstream boundary-layer mass flow was obtained for the 15° cone at $M_\infty = 3.78$ with one row of 54 0.064-in.-diam bleed holes. The holes were located at a cross section where the pressure ratio was about 2.7. The bleed plenum pressure was sufficiently low to ensure choked flow through the bleed holes. The flow patterns and surface static-pressure distribution (Fig. 10) indicate that the flow remained attached through the interaction region, whereas the flow was separated at the same conditions with zero suction. The multiple shock-wave pattern of the zero suction case (shown as dashed lines) was reduced to a single reflected shock similar to that obtained for unseparated interactions without suction, and the upstream spreading of the surface static-pressure rise was reduced by about 40%. Similar results were obtained for an equal suction flow rate with the perforations located upstream of the pressure rise[9]; however, four times as many bleed holes were required to obtain the necessary flow rate. When suction was applied for the 15° cone, the reduction in the boundary-layer thickness relative to the solid-wall case allowed the expansion from the base of the cone to pass downstream of the intersection of the reflected shock and the boundary-layer edge. The influence of the expansion on the flow patterns and boundary-layer properties immediately downstream of the interaction regions is, therefore, believed to be negligible for the perforated-wall tests. Results similar to those presented for 3.1% suction were obtained for suction

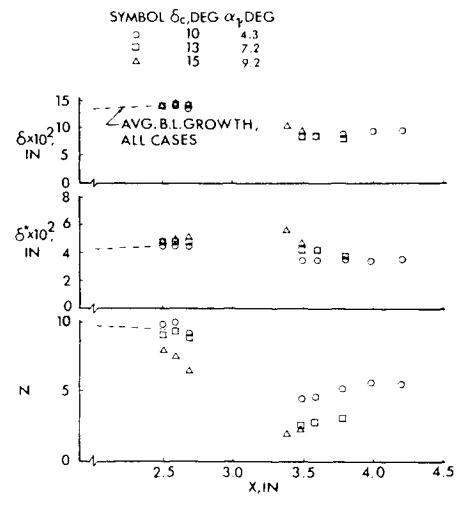

Fig. 8 Boundary-layer properties, $M_\infty = 3.78$.

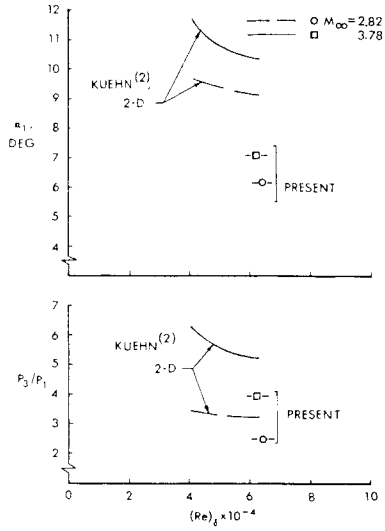

Fig. 9 Conditions for incipient separation.

rates up to 13.1% of the mass flow of the upstream boundary layer.

Boundary-layer properties

The boundary-layer properties downstream of the interaction region for the 15° cone with and without suction may be compared in Fig. 11. The x coordinates for the flows with suction were adjusted to superimpose the incident shock waves. The results with 3.1% suction indicate a significant improvement, in terms of reduced δ and increased N, in the characteristics of the boundary layer relative to the separated zero-suction case. The differences decrease rapidly with distance, however, as the expansion from the base of the cone causes the flow to accelerate. Additional improvements in the boundary-layer characteristics downstream of the interaction region were obtained by increasing the suction flow rate.

3. Comparison to Theory

3.1 Solid-Wall Tests

The results of theoretical calculations are compared to experimental data for all solid-wall tests in Fig. 12. The theoretical curves were determined using the analysis of Ref. 1 for average values of the upstream boundary-layer thickness and mass-flow equivalent power-law exponent for all data obtained at Mach 3.78. The two points to the left of the vertical dashed lines represent unseparated flows, whereas the three remaining flows exhibited characteristics of separated interactions with the accompanying upstream spreading of the static-pressure rise.

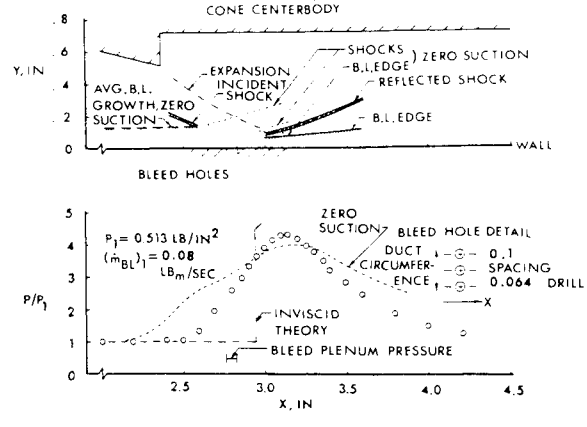

Fig. 10 Flowfield and surface static-pressure distribution for 15° cone at M_∞ = 3.78, 3.1% suction.

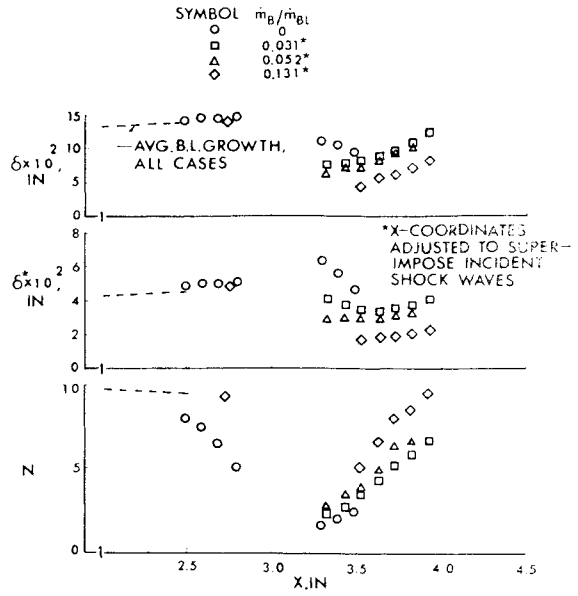

Fig. 11 Boundary-layer properties, 15° cone at M_∞ = 3.78.

The agreement between theoretical and experimental results is considered to be good (within 20%) for the unseparated interactions for which the flow models of the analysis of Ref. 1 were derived. The differences between analysis and experiment increase markedly with increasing shock strength when the experimental data exhibit characteristics indicative of separated flow. For these cases, the geometry of the flow models of Ref. 1 is no longer similar to the actual interaction. The good agreement obtained for the boundary-layer edge Mach number indicates that the assumption of a conical streamline boundary between the incident and reflected shocks[1] properly accounts for the difference between

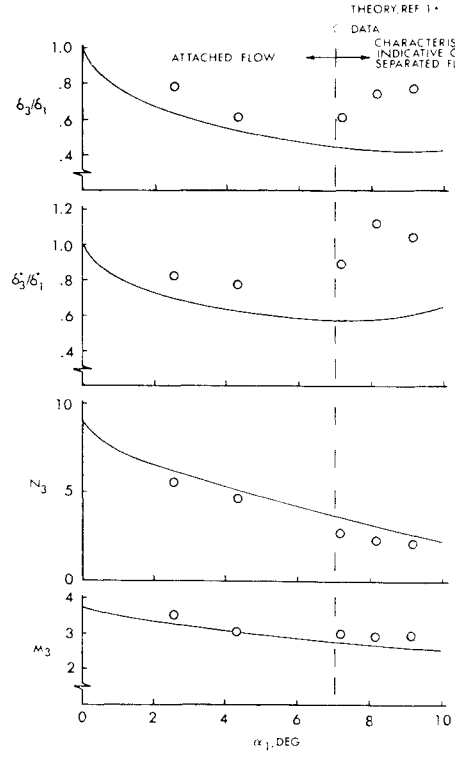

Fig. 12 Comparison of theory and experiment, M_∞ = 3.78 with solid wall.

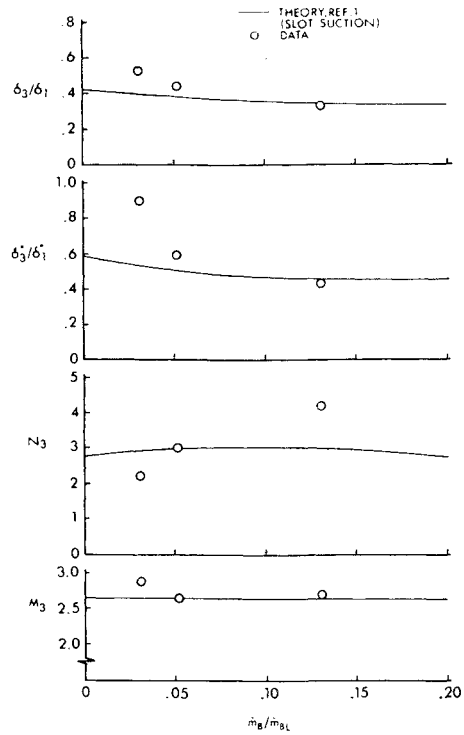

Fig. 13 Comparison of theory and experiment, 15° cone at $M_\infty = 3.78$ with perforated wall.

two-dimensional and axially symmetric external flows for the cases presented in this paper.

3.2 Perforated-Wall Tests

Comparisons of predictions made with the slot-suction flow model of Ref. 1 and experiment for the 15° cone are shown in Fig. 13 for three suction-flow rates. The upstream properties for the theoretical results correspond to the average values obtained for all cases with zero suction. Removal of 3.1% of the boundary-layer mass flow prevented separation but did not completely eliminate the upstream spreading of the surface static-pressure rise. At higher suction rates, the flow model more closely describes the flow patterns obtained experimentally. The agreement between theory and experiment for all boundary-layer properties improves with increasing suction flow rate. The agreement was good for the external flow parameter M_3 over the range of suction rates tested.

4. Conclusions

The results presented in this paper support the following conclusions.

1) The additional adverse pressure gradients present in axially symmetric flow reduce the shock wave strength at which separation is initially observed relative to results for two-dimensional flow, as reported by Kuehn,[2] when the same criterion for incipient separation is used for the comparison. The identification of a hump in the surface static-pressure distribution does not appear to be a reliable indication of completely attached flow for the present tests since in some instances characteristics indicative of separated flow with important changes in the flow pattern were observed before the appearance of a hump in the pressure distribution.

2) The observable effects of separation may be completely eliminated for separations as long as two boundary-layer thicknesses in extent by removing a small portion of the boundary-layer mass flow from the interaction region.

3) The power-law velocity profile was found to provide a good representation of the measured boundary-layer velocity distributions upstream of the incident shock waves and immediately downstream of the interaction regions for unseparated interactions. The predictions of Ref. 1 are in good agreement with the experimental results for interactions without extensive upstream spreading of the surface static-pressure rise.

4) Suction within the interaction region was more effective in suppressing the effects of separation for supersonic inlet applications than suction ahead of the shock impingement location when the problem of removal of the low pressure bleed flow was considered. This is in agreement with the discussion of Ref. 5, but not with the conclusions reached by Strike and Rippey.[3] The observations of the present study regarding the location of bleed perforations are also supported by the results of tests of a high-performance axially symmetric inlet.[10]

References

[1] Seebaugh, W. R., Paynter, G. C., and Childs, M. E., "Shock-Wave Reflection from a Turbulent Boundary Layer with Mass Bleed," *Journal of Aircraft*, Vol. 5, No. 5, Sept.-Oct. 1968, pp. 461–467.

[2] Kuehn, D. M., "Experimental Investigation of the Pressure Rise Required for the Incipient Separation of Turbulent Boundary Layers in Two-Dimensional Supersonic Flow," Memo. 1-21-59A, Feb. 1959, NASA.

[3] Strike, W. T. and Rippey, J., "Influence of Suction on the Interaction of an Oblique Shock with a Turbulent Boundary Layer at Mach Number 3," TN 61-129, Oct. 1961, Arnold Engineering Development Center.

[4] Kutschenreuter, P. H., Zurschmeide, R. L., and Surber, L. E., "An Investigation of Shock Wave-Boundary Layer Interaction with Suction," ASRMFD TM 61-30, Jan. 1962, U. S. Air Force.

[5] Wainwright, J. B., "Description of an Experimental Investigation of the Effects of Boundary Layer Bleed on Shock Wave-Boundary Layer Interaction," Rept. 65-35, Dec. 1962 Univ. of Southern California.

[6] Beitler, S. R., *Fluid Meters Their Theory and Application*, 5th ed., New York, 1959, American Society of Mechanical Engineers.

[7] Bogdonoff, S. M., Kepler, C. E., and Sanlorenzo, E., "A Study of Shock Wave Turbulent Boundary Layer Interaction at M = 3.0," Rept. 222, July 1953, Dept. of Aeronautical Engineering, Princeton Univ.

[8] Pinckney, S. Z., "Semiempirical Method for Predicting Effects of Incident-Reflecting Shocks on the Turbulent Boundary Layer," TN D-3029, Oct. 1965, NASA.

[9] Seebaugh, W. R., "An Investigation of the Interaction of a Shock Wave and a Turbulent Boundary Layer in Axially Symmetric Internal Flow Including the Effects of Mass Bleed," PhD thesis, 1968, Univ. of Washington.

[10] Cubbison, R. W., Meleason, E. T., and Johnson, D. F., "Effect of Porous Bleed in a High-Performance Axisymmetric, Mixed-Compression Inlet at Mach 2.50," TM X-1692, Nov. 1968, NASA.